Microsc. Microanal. 14, 60–67, 2008
DOI: 10.1017/S1431927608080148

Microscopy AND Microanalysis

© MICROSCOPY SOCIETY OF AMERICA 2008

High-Resolution TEM and the Application of Direct and Indirect Aberration Correction

Crispin J.D. Hetherington,[1] Lan-Yun Shery Chang,[1] Sarah Haigh,[1] Peter D. Nellist,[1] Lionel Cervera Gontard,[2,†] Rafal E. Dunin-Borkowski,[2,†] and Angus I. Kirkland[1,*]

[1]*Department of Materials, University of Oxford, Parks Road, Oxford OX1 3PH, UK*
[2]*Department of Materials Science and Metallurgy, University of Cambridge, Pembroke Street, Cambridge CB2 3QZ, UK*

Abstract: Aberration correction leads to a substantial improvement in the directly interpretable resolution of transmission electron microscopes. Correction of the aberrations has been achieved electron-optically through a hexapole-based corrector and also indirectly by computational analysis of a focal or tilt series of images. These direct and indirect methods are complementary, and a combination of the two offers further advantages. Materials characterization has benefitted from the reduced delocalization and higher resolution in the corrected images. It is now possible, for example, to locate atomic columns at surfaces to higher accuracy and reliability. This article describes the JEM-2200FS in Oxford, which is equipped with correctors for both the image-forming and probe-forming lenses. Examples of the use of this instrument in the characterization of nanocrystalline catalysts are given together with initial results combining direct and indirect methods. The double corrector configuration enables direct imaging of the corrected probe, and a potential confocal imaging mode is described. Finally, modifications to a second generation instrument are outlined.

Key words: aberration correction, nanocrystalline catalysis, confocal imaging, exit-wavefunction reconstruction

Introduction

The atomic structure of materials and defects are now routinely characterized at atomic resolution by high resolution transmission electron microscopy (HRTEM). In recent years, instrumental developments, including field emission sources, improved stability in accelerating voltage, and lens supplies, and stable goniometers have contributed to improved resolution. In combination these have allowed medium-voltage (200–300 kV) microscopes to record structural *information* at resolutions at or below 0.1 nm.

The ability to interpret images directly is, however, better indicated by the point resolution that, for an uncorrected microscope, typically lies in the 0.15–0.20-nm range. Information in the image is transferred beyond this limit, but with phase shifts introduced by the objective lens. The resulting delocalization associated with uncorrected aberrations also leads to difficulties in image interpretation, particularly for aperiodic features such as surfaces and interfaces. However, the point resolution is largely determined by the spherical aberration of the objective lens. Hence, the recent development of aberration correction has had an enormous impact on HRTEM.

Aberration correction can be achieved through either direct or indirect methods. Direct methods for HRTEM involve the insertion of multipole elements below the objective lens that correct the inherent positive spherical aberration (Scherzer, 1947). Indirect methods require a focal or tilt series of images, from which the aberrations may be measured and computationally compensated *a posteriori* to recover the specimen exit wavefunction (see Kirkland & Meyer, 2004, for a review). Off-axis holography using an electrostatic biprism offers an alternative route to recovering the exit wavefunction (Lichte, 1991).

In this article, we first outline the above two approaches to aberration correction and subsequently discuss the merits of applying them in combination. Examples obtained on the aberration-corrected JEM-2200FS formerly installed in Oxford are described. Correction of the probe-forming lens is also possible on this instrument, paving the way for confocal microscopy; initial results are also outlined. Finally, recent upgrades to this instrument are described.

Direct Aberration Correction

A JEOL 200-kV FEG(S)TEM with both probe and imaging aberration correctors and an in-column energy filter was installed in Oxford in 2003. This instrument (Fig. 1) was

Received June 29, 2007; Accepted August 7, 2007.
†Now at: Centre for Electron Nanoscopy, Technical University of Denmark, DK-2800 Kongens Lyngby, Denmark
**Corresponding author*. E-mail: angus.kirkland@materials.ox.ac.uk

Figure 1. The Oxford JEM-2200FS.

based on a JEM-2200FS (Hutchison et al., 2005; Sawada et al., 2005). The correctors are supplied by CEOS GmbH based on a design due to Rose and Haider (Haider et al., 1998*a*) in which the corrector elements consist of a pair of strong hexapoles and two round-lens doublets. As detailed elsewhere (Haider et al., 1998*b*; Lentzen, 2006), the primary aberration (a strong threefold astigmatism) of the first hexapole is compensated by the second hexapole in an antisymmetric configuration. This long hexapole arrangement generates a combination aberration that compensates the positive spherical aberration of the objective lens through suitable hexapole excitation. Additional weak multipole elements are also included for the adjustment of the beam axis and correction of parasitic aberrations to third order. The interpretable resolution is thus extended from 0.19 nm in the uncorrected state ($C_s = 0.5$ mm) to less than 0.12 nm in the corrected state (Fig. 2). The resolution is then limited only by the temporal coherence determined by the chromatic aberration and energy spread ($\Delta E = 0.7$ to 1.0 eV, $C_C = 1.3$ mm).

In practice, adjustment of the imaging corrector is achieved through two or more steps. The coarse twofold astigmatism is first corrected using an untilted image of a thin amorphous film and the focus adjusted to a suitable underfocus (typically between 200 and 400 nm for images recorded at 300,000× magnification). Alignment then proceeds with the acquisition of a Zemlin tableau of diffractograms calculated from images of a thin amorphous foil recorded at several tilt azimuths with constant tilt magnitude (Zemlin et al., 1978; Zemlin, 1979). A tilt value of 18 mrad might typically be used initially for a coarsely aligned state, and a higher tilt value of 40 mrad is used for final

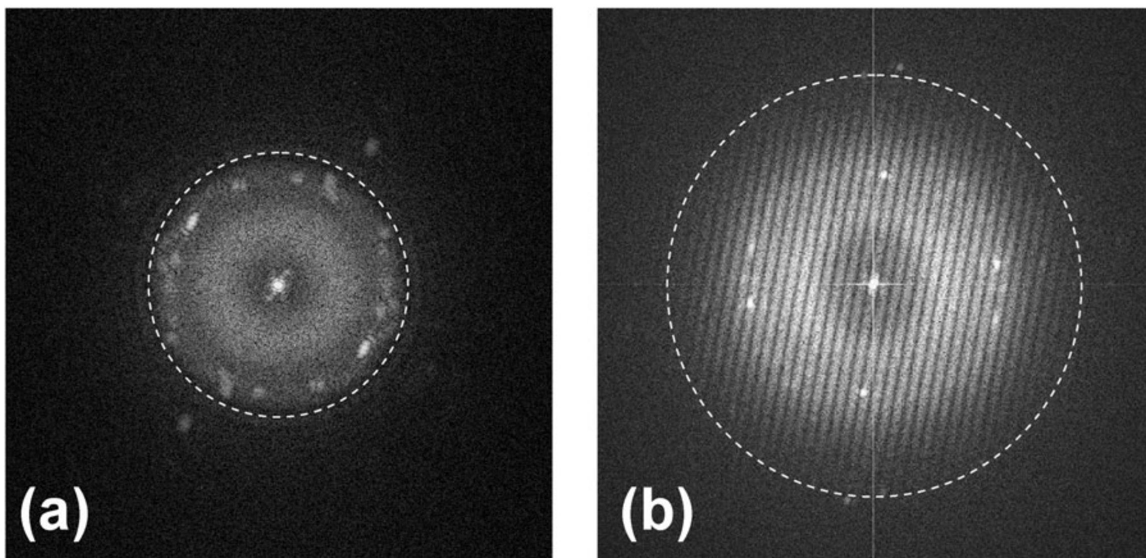

Figure 2. Power spectra calculated from images of a thin amorphous germanium film decorated with gold particles. **a:** $C_s = 0.5$ mm with point resolution limit at 0.19 nm indicated. **b:** $C_s = 0.0$ 1mm with resolution limit at 0.12 nm indicated.

correction of the higher order aberrations. These data sets are used to measure the tilt-induced defocus and twofold astigmatism, which provide linear estimates for the coefficients of the wave aberration function. To accomplish the measurement, Uhlemann and Haider (1998) have developed a computationally efficient algorithm in which each experimental diffractogram is compared to a library of precalculated diffractograms. Finally, the estimated coefficients of the aberration function are used to automatically adjust the corrector currents. In practice, the spherical aberration and other aberration coefficients may be set to zero for pure amplitude contrast, or the spherical aberration coefficient may be set to a small negative value for optimum phase contrast (Lentzen et al., 2002; Chang et al., 2003). It is good practice to record values of the coefficients (including the error in each) as calculated from the Zemlin tableau both before and after the acquisition of experimental images. These values may also subsequently be used in post-acquisition analysis, as described later.

Indirect Aberration Compensation

Several methods have been developed for experimental determination of the axial aberration coefficients (e.g., Kirkland et al., 2006). All are based on the injection of known beam tilts and the measurement of one of several possible observables in the image. Historically, image displacements as a function of beam tilt have been measured through standard cross-correlation functions (e.g., Typke & Dierksen, 1995), but the utility of this approach is, in practice, restricted to coarse alignments. Alternatively, the measurement of diffractograms of thin amorphous materials (Kirkland et al., 1995; Coene et al., 1996) reveal the tilt-induced defocus and astigmatism from which the coefficients may be calculated.

The final method relies on measurements taken from image wavefunctions (Meyer et al., 2002, 2004) and is applicable to crystalline specimens as well as thin amorphous materials. Initially, a phase correlation function (PCF) (Kuglin & Hines, 1975) is used to determine the defocus difference between neighboring images to high accuracy. The absolute focus and astigmatism are subsequently measured from the restored image wavefunction of a reference image using a phase contrast index (PCI) function.

All of the above indirect methods provide estimates of the coefficients of the wave aberration function, which can subsequently be used to recover both the phase and modulus of the specimen exit wavefunction (Saxton, 1988) under either linear or nonlinear imaging. This provides resolution enhancement for uncorrected microscopes, but can also complement direct aberration correction, as described in the next section.

Combining Direct and Indirect Methods

Direct electron-optical correction offers the advantage that it may be achieved online in a single image, with no requirement for postacquisition processing or acquisition of extended focal or tilt azimuth series. However, with current generation optical elements, correction of aberrations extends to the third order only, and the recorded data comprises intensity only.

Indirect correction or compensation of aberrations has the primary advantage that the complex exit wavefunction is reconstructed. Correction to any order is theoretically possible, limited only by the measurement accuracy, and the process is achieved through relatively simple software. The disadvantage is that this is necessarily an off-line technique requiring multiple image data sets, although faster computers and appropriate adaptation of software should soon allow reconstructions to be achieved at the microscope in close to real time.

Indirect and direct approaches have been used in combination (Tillmann et al., 2004) and provide additional advantages. For a focal-series data set, the elimination of tilt-induced axial coma relaxes the requirement of using parallel illumination and enables the illumination to be converged onto the specimen area of interest. Current density at the sample may be maintained in this manner while reducing the emitter current, thereby giving a reduced energy spread in the illumination (for a Schottky source), and hence an improved information limit. For a tilt-series data set, the elimination of tilt-induced axial coma gives rise to less critical focus conditioning for a given tilt magnitude (Kirkland et al., 1995) and multiple tilt magnitudes are possible without any induced focus change. For either geometry, the reduced delocalization of image components in the electron-optically corrected image is advantageous. The voltage center and axial coma-free axis are also coincident, and hence the temporal coherence envelope is symmetric, and localized compensation of higher order aberrations up to the fifth order is also possible. Finally, we note that the beam tilt coils may be used for precise sample axis alignment about a limited range because all axes are free of axial coma.

Experimentally, 20-member focal series about Gaussian focus are typically taken with focal increments of 5–10 nm with the spherical aberration adjusted to a small negative value. Images in the focal series are preprocessed to account for the effects of the camera modulation transfer function and noise power spectrum (Meyer et al., 2000) prior to recovery of the specimen exit wavefunction. Figure 3 illustrates typical phase plates obtained after initial electron-optical correction to the third order, and after aberration refinement to the fifth order using locally determined values of the aberration coefficients (Kirkland et al., 2006), with the latter clearly showing a clear improvement in the extent of transfer within a $\pi/4$ phase limit.

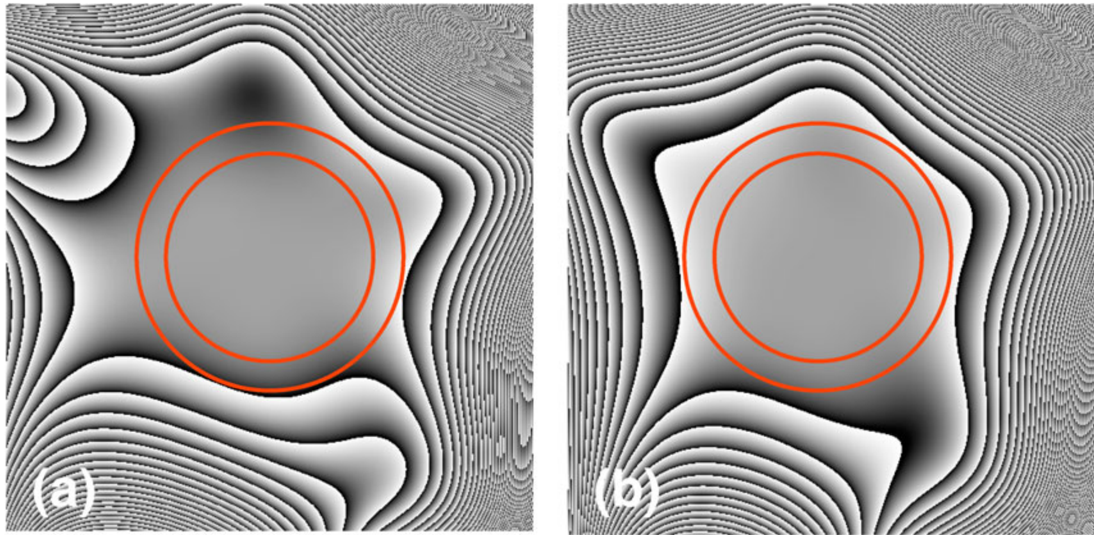

Figure 3. Phase plates calculated to the fifth order from residual aberrations. **a:** After direct electron optical correction to the third order. **b:** After local refinement of aberrations to the third order using the PCF/PCI method. Black to white represents a phase shift of π. Inner and outer circles represent resolution limits of 0.1 and 0.08 nm.

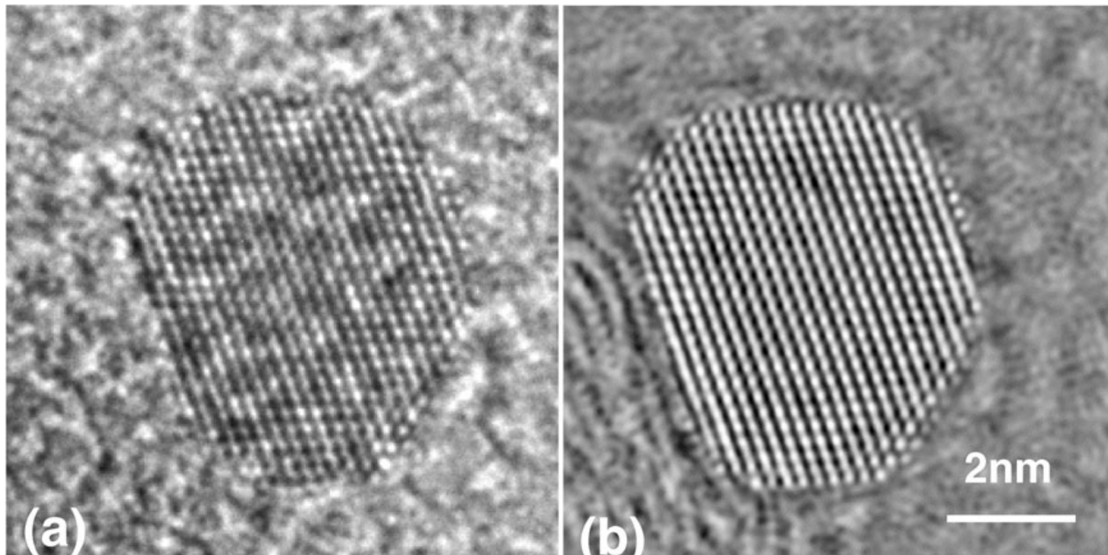

Figure 4. a: Aberration-corrected image of Pt nanoparticle taken from a series of 20 images ($\Delta f = -93$ nm, $C_s = -30$ μm). **b:** Phase of restored specimen exit wavefunction.

Applications

Two applications are described illustrating the benefits of combining direct and indirect aberration correction to HRTEM.

Figure 4a shows a Pt nanoparticle oriented close to a ⟨110⟩ direction supported on partially graphitized carbon. This image forms part of a 20-member focal series acquired at 200 kV with 5-nm focal steps and with the spherical aberration adjusted to -30 μm (Cervera Gontard et al., 2007). Restoration of the specimen exit wavefunction reveals substantially more structural detail in the restored phase (Fig. 4b) with surface monatomic steps, adatoms, and localized rearrangements clearly visible. The graphitic planes of the support are also resolved in the reconstructed phase, and a partial epitaxial contact between a graphene sheet and a {111} facet can be seen, in agreement with previous studies of Ni{111} surfaces (Eizenberg & Blakely, 1979).

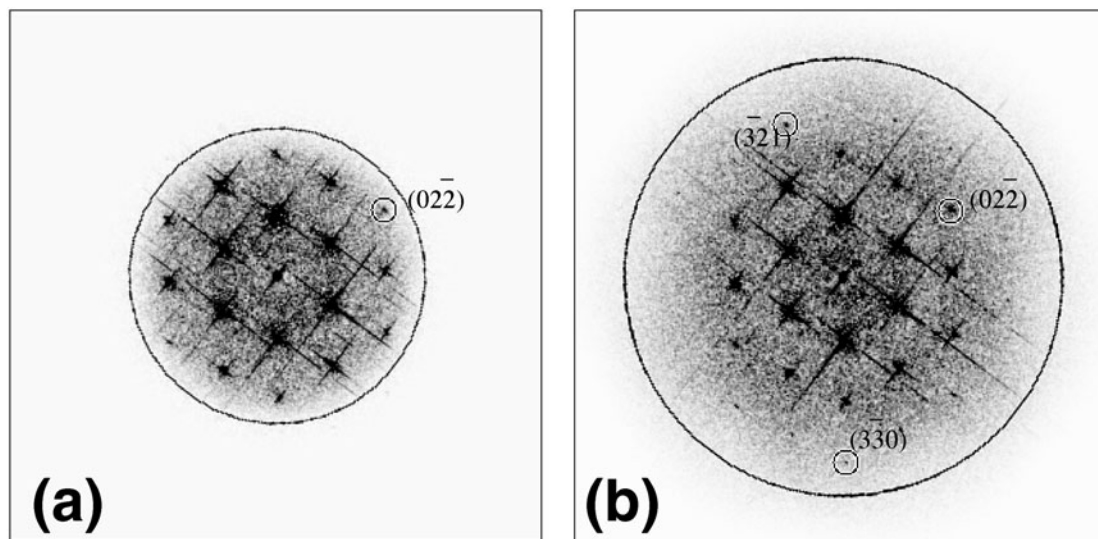

Figure 5. Moduli of Fourier transforms of the complex specimen exit wavefunctions of ⟨111⟩ orientated $SrTiO_3$ using (**a**) focal-series data and (**b**) combined tilt/focal-series data. Circles indicate the limit for which information transfer drops below 10%, equivalent to a spatial resolution of 0.12 nm for the focal series and 0.08 nm for the tilted data set. Selected high-order reflections are highlighted to emphasize the presence of additional information in the exit wavefunction recovered from the tilt/focal-series data compared to the axial focal series data.

In the second example, images of thin crystals of ⟨111⟩ oriented $SrTiO_3$ were examined in order to compare indirect aberration compensation using focal- and tilt-series data set geometries (Haigh et al., 2006). Experimental focal series comprised 20 images separated by a focal increment of 10 nm with the series centered about the Gaussian focus condition with a typical spherical aberration of $-3\ \mu$m. Tilt series consisted of six short focal series taken at different illumination tilt directions using tilt magnitudes of up to 20 mrad.

For both data sets, specimen exit wavefunctions were restored under the same linear imaging approximation. Aberrations were initially measured to the fifth order from diffractograms and electron-optically corrected to the third order. Subsequently the aberrations were locally refined to the fifth order for a specimen subregion of interest using the PCF/PCI approach to an accuracy of <1 nm.

Figure 5 demonstrates the improvement in information transfer that can be obtained using a tilt-series data set for exit wavefunction restoration. The exit wavefunction restored from the focal series shows information transfer (at 10%) corresponding to a resolution of 0.12 nm, whereas the same level of information transfer limit is extended to 0.08 nm in the tilt-series reconstruction.

Double Correction

It is important to note the consequences on microscope operation of the double corrector arrangement. For experiments in which only HRTEM data are required, the upper corrector may be switched off and the condenser system of the JEM-2200FS can then be used as normal. In practice, a small voltage is applied to one of the hexapoles in the upper corrector to compensate for a residual threefold astigmatism arising from the gun lens and any residual field from the first hexapole. For experiments in which a small probe is required for analysis or STEM imaging in combination with HRTEM imaging, it is preferable to leave the upper hexapoles excited in order to avoid the effects of hysteresis while the hexapole fields stabilize. To achieve this arrangement, a small adjustment to transfer lenses in the upper corrector is possible that allows broad parallel illumination to be achieved satisfactorily with both upper hexapoles strongly excited.

A novel use of double correction is for three-dimensional imaging and analysis. The depth of focus of a lens is inversely proportional to the square of its numerical aperture, and aberration correction in TEM can lead to depths of focus of only a few nanometers. In STEM, this reduced depth of focus has been used to optically section samples and to reconstruct three-dimensional images (Van Benthem et al., 2005). In the JEM-2200FS, correction of both pre- and postfield allows the use of large condenser and objective aperture sizes and hence the possibility of using the instrument as a scanning confocal electron microscope (Nellist et al., 2006). To align the instrument in a confocal configuration, both the pre- and postfield correctors must be simultaneously optimized. If the postspecimen optics are used to form a diffraction pattern, then a Ronchigram is observed (Lin & Cowley, 1986; Fig. 6), from which the

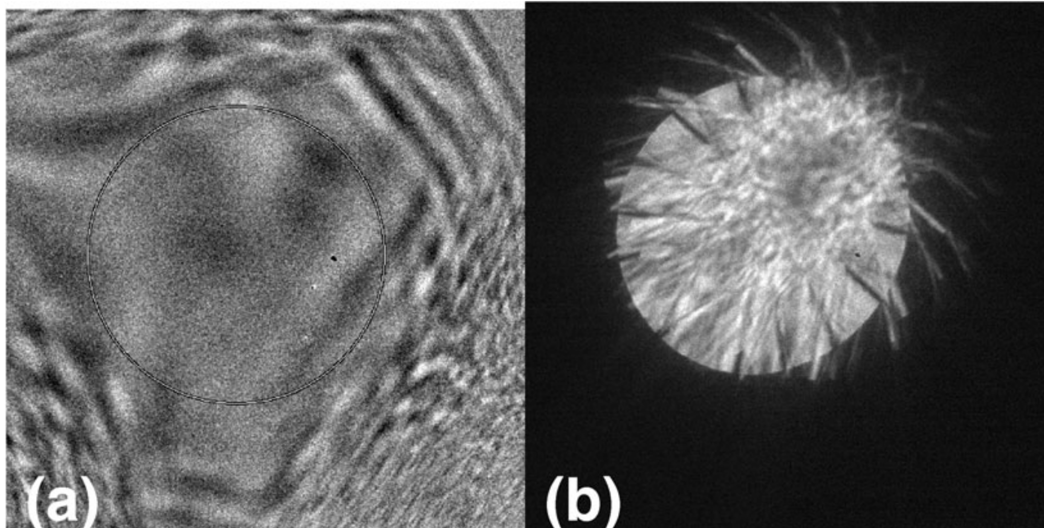

Figure 6. **a:** Ronchigram of amorphous carbon film with radius of 30 mrad marked. **b:** Kikuchi bands from a thick silicon crystal in a ⟨110⟩ orientation allowing camera length calibration and measurement of a (noncircular) condenser aperture size between 56 and 60 mrad diameter. (Reproduced from *Appl Phys Lett* **89**, 124105, copyright 2006, American Institute of Physics.)

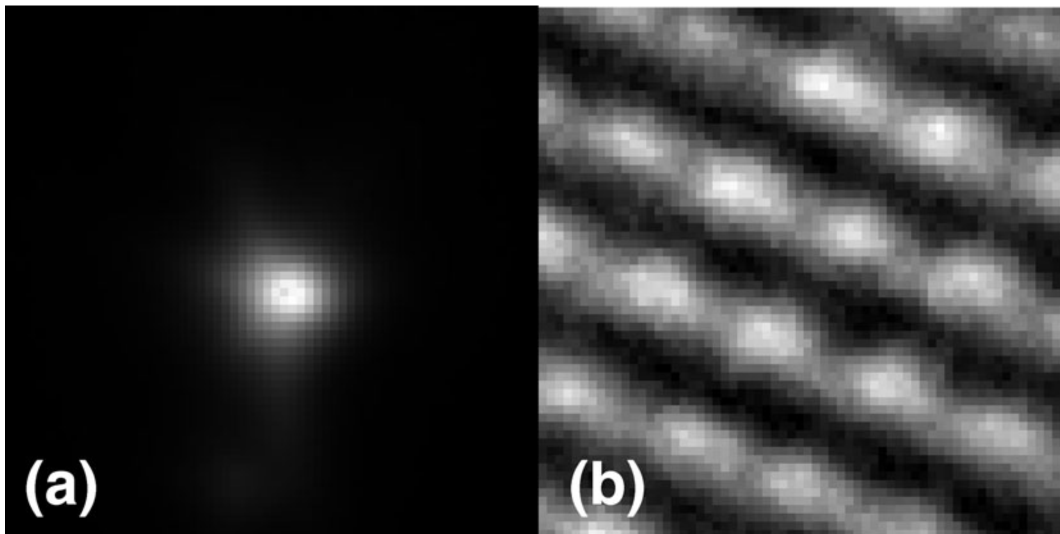

Figure 7. **a:** Image of a probe formed with the microscope in confocal configuration, with average FWHM of 0.17 nm. **b:** Silicon single crystal imaged along ⟨110⟩ direction at the same magnification, which serves as the calibration. (Reproduced from *Appl Phys Lett* **89**, 124105, copyright 2006, American Institute of Physics.)

probe-forming optics can be tuned. Imaging mode then allows a magnified image of the probe to be formed (Fig. 7). If the probe-forming optics are corrected, any distortions in the image can be described by postfield aberrations and the postfield corrector tuned by observation of the probe shape. Hence, with both correctors tuned it is possible to establish confocal trajectories in the microscope.

Future Developments

Aberration correction in HRTEM has brought the point resolution beyond the 0.1-nm level, limited only by the chromatic aberration and temporal coherence. If the microscope is sufficiently mechanically stable to allow longer

exposure times, then the emission may be reduced, with a consequent reduction in energy spread in the beam from around 1 eV to 0.5 eV for a Schottky source without monochromation. For these values, the resolution, measured as the spacing at which the transfer drops to a 10% value, improves from 0.12 nm to 0.10 nm at 200 kV. It is planned to add a double Wien filter monochromator to our second generation microscope (Mukai et al., 2005), which will allow the use of energy spreads as low as 0.2 eV for HRTEM observations. Mechanical improvements, including an isolating cover for the specimen holder and remote operation from an adjacent room, are among provisions to allow longer exposure times and reduced drift of the sample during the acquisition of focal or tilt series that typically comprise between 20 and 27 images. To realize the full benefit of the reduced energy spread, the power supplies for HT and objective lens have ripples of less than 0.5 ppm, and a piezo drive for specimen height control will facilitate the collection of through focal series of images without the need to alter the objective lens excitation and will be essential for scanning confocal electron microscopy experiments. Aberration correction of the objective lens prefield results in higher beam currents and smaller probes: the acquisition of the resulting intense probe images on the CCD is hindered by saturation effects. This has been addressed by two fast piezo shutters (above and below the objective lens) and by increased magnification of the projector system below the omega filter.

Acknowledgments

The JEM-2200FS and subsequent developments have been funded by the UK Engineering and Physical Sciences Research Council with support from JEOL Ltd.

References

Cervera Gontard, L., Chang, L.-Y., Hetherington, C.J.D., Kirkland, A.I., Ozkaya, D. & Dunin-Borkowski, R.E. (2007). Aberration-correction imaging of active sites on industrial catalyst nanoparticles. *Angew Chem* **46**, 3683–3685.

Chang, L.-Y., Chen, F.-R., Kirkland, A.I. & Kai, J.J. (2003). Calculations of spherical aberration-corrected imaging behaviour. *J Electron Microsc* **52**, 359–364.

Coene, W.M.J., Thust, A., Op De Beeck, M. & Van Dyck, D. (1996). Maximum-likelihood method for focus-variation image reconstruction in high resolution transmission electron microscopy. *Ultramicroscopy* **64**, 109–135.

Eizenberg, M. & Blakely, J.M. (1979). Carbon interaction with nickel surfaces: Monolayer formation and structural stability. *J Chem Phys* **71**, 3467–3477.

Haider, M., Rose, H., Uhlemann, S., Kabius, B. & Urban, K. (1998*a*). Electron microscopy image enhanced. *Nature* **392**, 768–769.

Haider, M., Rose, H., Uhlemann, S., Schwan, E., Kabius, B. & Urban, K. (1998*b*). A spherical aberration corrected 200kV transmission electron microscope. *Ultramicroscopy* **75**, 53–60.

Haigh, S., Kirkland, A.I. & Chang, L.Y. (2006). Aberration corrected tilt series reconstruction. In *Proceedings of 16th International Microscopy Congress, Sapporo*. Ichinose, H. & Sasaki, T. (Eds.), p. 943. Sapporo, Japan: Japanese Society for Electron Microscopy.

Hutchison, J.L., Titchmarsh, J.M., Cockayne, D.J.H., Doole, R.C., Hetherington, C.J.D., Kirkland, A.I. & Sawada, H. (2005). A versatile double aberration-corrected, energy filtered TEM/STEM for materials science. *Ultramicroscopy* **103**, 7–15.

Kirkland, A.I. & Meyer, R.R. (2004). "Indirect" high-resolution transmission electron microscopy: Aberration measurement and wavefunction reconstruction. *Microsc Microanal* **10**, 401–413.

Kirkland, A.I., Meyer, R.R. & Chang, L.-Y.S. (2006). Local measurement and computational refinement of aberrations for HRTEM. *Microsc Microanal* **12**, 461–468.

Kirkland, A.I., Saxton, W.O., Chau, K.L., Tsuno, K. & Kawasaki, M. (1995). Super-resolution by aperture synthesis: Tilt series reconstruction in CTEM. *Ultramicroscopy* **57**, 355–374.

Kuglin, C.D. & Hines, D.C. (1975). The phase correlation image alignment method. In *Proceedings of the IEEE International Conference on Cybernetics and Society*, pp. 163–165. New York: IEEE.

Lentzen, M. (2006). Progress in aberration-corrected high-resolution transmission electron microscopy using hardware aberration correction. *Microsc Microanal* **12**, 191–205.

Lentzen, M., Jahnen, B., Jia, C.L., Thust, A., Tillmann, K. & Urban, K. (2002). High-resolution imaging with an aberration-corrected transmission electron microscope. *Ultramicroscopy* **92**, 233–242.

Lichte, H. (1991). Electron image plane off-axis holography of atomic structures. *Adv Opt Elect Microsc* **12**, 25.

Lin, J.A. & Cowley, J.M. (1986). Calibration of the operating parameters for an HB5 STEM instrument. *Ultramicroscopy* **19**, 31–42.

Meyer, R.R., Kirkland, A.I., Dunin-Borkowski, R.E. & Hutchison, J.L. (2000). Experimental characterization of CCD cameras for HREM at 300kV. *Ultramicroscopy* **85**, 9–13.

Meyer, R., Kirkland, A. & Saxton, W. (2002). A new method for the determination of the wave aberration function for high resolution TEM. 1. Measurement of the symmetric aberrations. *Ultramicroscopy* **92**, 89–109.

Meyer, R., Kirkland, A. & Saxton, W. (2004). A new method for the determination of the wave aberration function for high resolution TEM. 2. Measurement of the antisymmetric aberrations. *Ultramicroscopy* **99**, 115–123.

Mukai, M., Kaneyama, T., Tomita, T., Tsuno, K., Terauchi, M., Tsuda, K., Naruse, M., Honda, T. & Tanaka, M. (2005). Performance of a new monochromator for a 200 kV analytical electron microscope. *Microsc Microanal* **11**(Suppl. 2), 2134–2135.

Nellist, P.D., Behan, G., Kirkland, A.I. & Hetherington, C.J.D. (2006). Confocal operation of a transmission electron microscope with two aberration correctors. *Appl Phys Lett* **89**, 124105.

Sawada, H., Tomita, T., Naruse, M., Honda, T., Hambridge, P., Hartel, P., Haider, M., Hetherington, C., Doole, R., Kirkland, A., Hutchison, J., Titchmarsh, J. & Cockayne, D. (2005). Experimental evaluation of a spherical aberration-corrected TEM and STEM. *J Electron Microsc* **54**, 119–121.

Saxton, W.O. (1988). Accurate atom positions from focal and tilted beam series of high resolution electron micrographs. In *Image and Signal Processing in Electron Microscopy. Proceedings of the 6th Pfefferkorn Conference, Niagara*, Hawkes, P.W., Ottensmeyer, F.P., Saxton, W.O. & Rosenfeld, A. (Eds.), pp. 213–224. Chicago: Scanning Microscopy International.

Scherzer, O. (1947). Sphärische und chromatische Korrektur von Elektronen-Linsen. *Optik* **2**, 114–132.

Tillmann, K., Thust, A. & Urban, K. (2004). Spherical aberration correction in tandem with exit-plane wave function reconstruction: Interlocking tools for the atomic scale imaging of lattice defects in GaAs. *Microsc Microanal* **10**, 185–198.

Typke, D. & Dierksen, K. (1995). Determination of image aberrations in high resolution electron microscopy using diffractogram and cross-correlation methods. *Optik* **99**, 155–166.

Uhlemann, S. & Haider, M. (1998). Residual wave aberrations in the first spherical aberration corrected transmission electron microscope. *Ultramicroscopy* **72**, 109–119.

Van Benthem, K., Lupini, A.R., Kim, M., Baik, H.S., Doh, S., Lee, J.-H., Oxley, M.P., Findlay, S.D., Allen, L.J., Luck, J.T. & Pennycook, S.J. (2005). Three-dimensional imaging of individual hafnium atoms inside a semiconductor device. *Appl Phys Lett* **87**, 034104.

Zemlin, F. (1979). A practical procedure for alignment of a high resolution electron microscope. *Ultramicroscopy* **4**, 241–245.

Zemlin, F., Weiss, K., Schiske, P., Kunath, W. & Herrmann, K.-H. (1978). Coma-free alignment of high resolution electron microscopes with the aid of optical diffractograms. *Ultramicroscopy* **3**, 49–60.